

Steam Catalytic Cracking of *n*-Dodecane to Light Olefins over Phosphorous- and Metal-Modified Nanozeolite Y

Emad N. Al-Shafei, Ahmad Masudi, Zain H. Yamani, and Oki Muraza*

Cite This: *ACS Omega* 2022, 7, 30807–30815

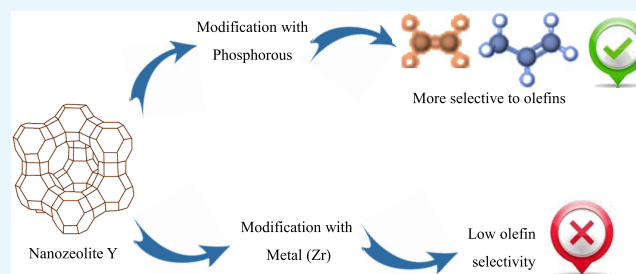
Read Online

ACCESS |

Metrics & More

Article Recommendations

ABSTRACT: Nanozeolite Y was synthesized without a template and modified with phosphorous (P) and metals. P was introduced via impregnation with different weight loadings (0.5, 1, and 2 wt %), while ion exchange was developed to introduce zirconium (Zr) and cobalt (Co). The physicochemical properties of the catalysts were characterized with X-ray diffraction (XRD), N₂ adsorption–desorption, temperature-programmed desorption of ammonia (NH₃-TPD), and ²⁷Al and ³¹P solid-state nuclear magnetic resonance (NMR). The parent nanozeolite Y showed an identical XRD pattern to that of a previous study, and the modified nanozeolite Y showed a lower crystallinity. The introduction of P altered tetrahedral Al to an octahedral coordination, which affected the catalyst acidity. Then, the catalyst was evaluated to produce olefins from *n*-dodecane at 550, 575, and 600 °C. The conversion, gas yield, and olefin yield increased with increasing temperature. The maximum olefin yield (63%) was achieved with the introduction of 1 wt % P with the highest selectivity to ethylene. The Co-modified nanozeolite altered the zeolite structure and exhibited similar activity to the P-modified one. Meanwhile, Zr-modified nanozeolite Y caused excessive metal distribution, blocked the porous structure of the zeolite, and then reduced the catalytic activity.



1. INTRODUCTION

Increasing global population and living standards have expanded the demand for chemicals, including olefins. Light olefins such as ethylene and propylene are essential feedstocks in polymer production, while butene is a backbone in styrene-butadiene manufacturing.¹ The main route for olefin production was steam cracking of petroleum, which consumed around 40% of energy in the petrochemical industry, as it operated above 750 °C.² The declining petroleum deposit and increasing public awareness to the petrochemical pollution motivated many researchers to develop cleaner technologies and alternative sources for olefin production.

Methane is one of the alternative feedstocks to olefins. Oxidative coupling of methane (OCM) is a direct production of olefins from methane. Nevertheless, this process is highly exothermic and challenging due to the reactor design and high investment. Another process was methanol to olefins (MTO) that produces olefins from methanol.³ However, MTO released 6–10 times CO₂ as compared to traditional naphtha crackers.⁴ Therefore, it is crucial to develop alternative processes to support worldwide initiatives to reduce the emission of greenhouse gases.

n-Dodecane is a long-chain paraffin that is generally used as an organic solvent in power plants.^{5,6} Additionally, dodecane was also reported as a jet fuel that could also be converted to other valuable chemicals such as hydrogen and light hydrocarbon.⁷ The conversion of long-chain hydrocarbons to lower

chains typically used zeolite as a catalyst. Even though the microporous zeolites show excellent activity, their performance for long-chain hydrocarbons was limited to slow mass transfer and rapid coking. This type of hydrocarbon required a large pore size and high surface area. There are some methods to hinder this limitation, namely, by modification to mesoporous zeolites,⁸ hierarchical zeolites,⁹ and nanozeolites.¹⁰ Konno et al. reported that nanosized zeolite was more stable in naphtha cracking with a higher olefin yield than micro-sized zeolite.¹¹ Additionally, the nanozeolite was also more efficient in several reactions such as methanol to hydrocarbon, acetone to olefins, and naphtha cracking.¹² Thus, these results triggered more studies on the potential of nanosized zeolite in catalytic cracking of heavy hydrocarbon.

To the best of our knowledge, there are only a few studies on *n*-dodecane cracking with nanozeolites. Ji et al.¹³ used ZSM-5 for dodecane cracking under supercritical conditions, which is challenging for commercialization. Meanwhile, Hao et al. utilized ITQ zeolite, but it requires high pressure to work

Received: April 5, 2022

Accepted: August 12, 2022

Published: August 23, 2022



efficiently.¹⁴ Zeolite Y is a potential catalyst in catalytic cracking due to its high acidity, porosity, and stability. Radman et al. synthesized nanozeolite Y in the absence of a template and found that the metal salt affected its size and pore characteristics.¹⁵ The *n*-dodecane catalytic cracking is an endothermic reaction, which is favorable at high temperatures. Previously, several studies have shown that the olefin selectivity of zeolite was enhanced by post-treatment with phosphorous¹⁶ and metals.¹⁷ In addition, Deng et al. reported that the cation position affected acidity and stability of the zeolite structure¹⁸ and previously reported that the zeolite acidity influenced the activation energy of hydrocarbon cracking.¹⁹ The introduction of Zr to zeolite Y increased Brønsted acid density and increased heavy oil conversion,²⁰ while incorporation of Co decreased the amount of coke.²¹ Previously, we have reported morphology–activity dependence in *n*-dodecane cracking.²² In this study, nanozeolite Y and modified nanozeolite Y with phosphorous and metals were synthesized without a template. The physicochemical properties of the catalysts were characterized. Then, these catalysts were evaluated to produce olefins from *n*-dodecane at several reaction temperatures.

2. EXPERIMENTAL SECTION

2.1. Catalyst Preparation and Characterization. The parent nanozeolite Y was synthesized without a template with

Table 1. Details of the Catalysts in this Study

catalyst names	details
P	parent zeolite for P modification
H-P	parent sample for metal modification
P1	P-modified with 0.5 wt % P
P2	P-modified with 1.0 wt % P
P3	P-modified with 2.0 wt % P
CoY	H-P ion exchange with 0.2 M Co
ZrY	H-P ion exchange with 0.2 M Zr

the following molar composition: 9 Na₂O: 0.7 Al₂O₃: 10 SiO₂: 160 H₂O. Sodium hydroxide (NaOH, Sigma Aldrich, 97%) was dissolved to 38% in water followed by addition of aluminum powder (Al, 325 mesh, Loba Chemie, >98%). This suspension was stirred at 700 rpm until completely dissolved

and named as aluminate solution. Meanwhile, the silicate solution was prepared by stirring 71 g of colloidal silica (Ludox-HS 30, Sigma Aldrich, 40 wt % SiO₂) with microwave irradiation at 100 °C. After that, the aluminate solution was added slowly to the silicate solution with a ratio of 10:1. This suspension was left for aging for 24 h at room temperature with stirring at 700 rpm. The suspension was then placed in an autoclave for hydrothermal treatment at 50 °C for another 24 h. Finally, the slurry was washed and centrifuged three times to ensure the removal of impurities and then dried overnight at 105 °C.

In this study, the as-prepared nanozeolites were modified with either addition of phosphorous (P) or metals. Various contents of P (0.5, 1, and 2 wt %) were added to the parent nanozeolite by the conventional impregnation method. A certain concentration of phosphoric acid was added to 15 mL of water containing 15 g of nanozeolite Y. The mixture was then dried at 110 °C for 5 h and calcined at 600 °C for 3 h. For metal modifications, the as-synthesized nanozeolite was calcined at 550 °C for 4 h to obtain protonated parent zeolite (H-P). The metal modification was carried out by dissolving 0.2 M Co(NO₃)₂(H₂O)₆ (Sigma Aldrich) or oxynitrate hydrate Zr(NO₃)₄ (Sigma Aldrich) to an aqueous solution of H-P (1 g in 30 mL of water) at 65 °C for 15 min. After that, the suspension was dried and calcined at 600 °C for 12 h. The details for the catalyst in this study are listed in Table 1. Thereafter, the crystallinity of the sample and catalyst acidity were identified with X-ray diffraction (XRD) and ammonia temperature-programmed desorption (NH₃-TPD). Then, the textural properties of the sample were elucidated with N₂ adsorption–desorption. The surface area and pore volume were determined with the Brunauer–Emmett–Teller (BET) model in the range of P/Po of 0.001–0.015 and 0.99, respectively. The pore size was calculated with the t-plot method. Lastly, the structures of Al and P were studied with solid-state nuclear magnetic resonance (NMR).

2.2. Catalytic Evaluation. The catalytic evaluation was carried out in a fixed-bed reactor as illustrated in Figure 1. Prior to the reaction, the catalyst was preheated under N₂ with a flow rate of 30 cm³/min for 1 h and used as a gas carrier during the reaction. *N*-dodecane and water were pumped to the reactor with a ratio of 9–1 and fixed liquid hourly space

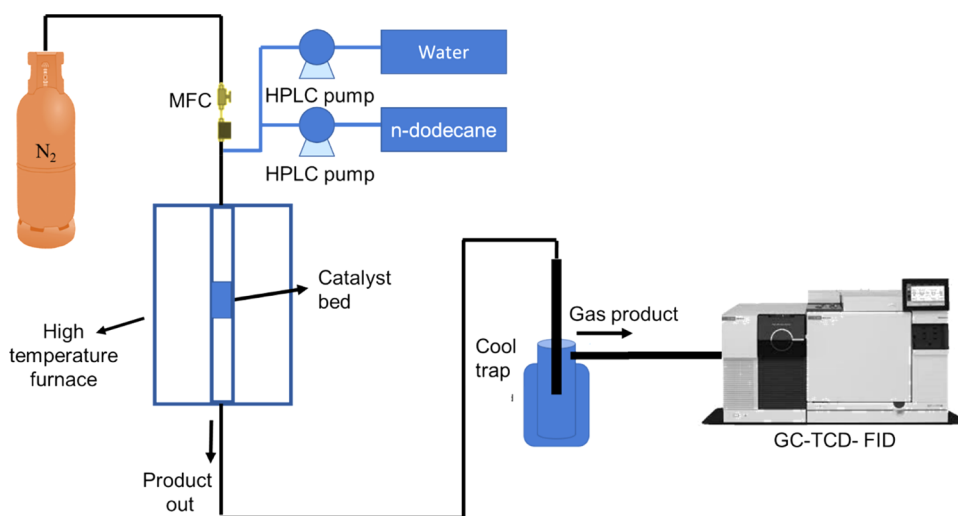


Figure 1. Schematic diagram of the catalytic studies.

velocity (LHSV) at 6 h^{-1} . The reaction was conducted at various temperatures (550, 575, and $600 \text{ }^\circ\text{C}$) for 120 min. Then, the effluent was sent to a cold trap ($-10 \text{ }^\circ\text{C}$) to separate the liquid and gas fractions. The gas was sent directly from the cold trap to the GC-RGA (GC-FID-TCD), and the liquid fraction was weighed, which contained the water and hydrocarbon layers. The hydrocarbon layer consists of converted and unconverted C12, which was then further analyzed with GC. The hydrocarbon conversion and selectivity were calculated, respectively, with eqs 1 and 2

$$C_{12} \text{ conversion (wt \%)} = 1 - \frac{C_{12_{\text{in}}}}{C_{12_{\text{out}}}} \times 100\% \quad (1)$$

$$\text{product selectivity (wt \%)} = \frac{\text{Product}}{C_{12_{\text{in}}} - C_{12_{\text{out}}}} \times 100\% \quad (2)$$

3. RESULTS AND DISCUSSION

3.1. Physicochemical Properties of the Catalysts.

Figure 2 shows the X-ray diffraction (XRD) pattern of the

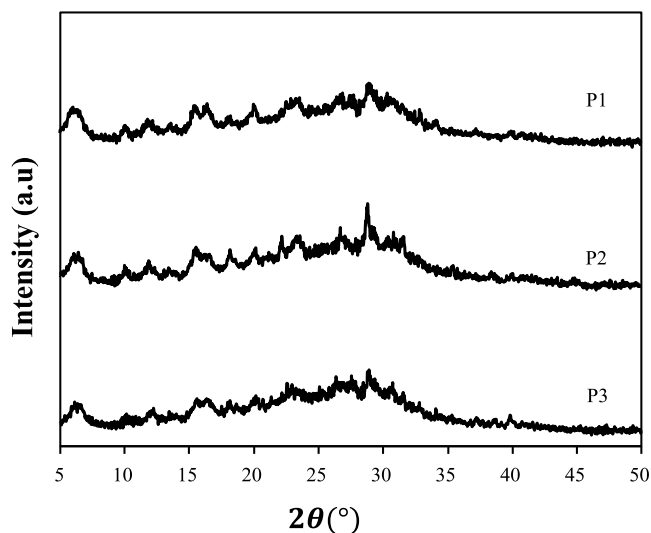


Figure 2. XRD pattern of phosphorous-modified nanozeolite Y with P1 (0.5 wt % P), P2 (1 wt % P), and P3 (2 wt % P).

catalyst after modification with P in a series of weight loadings (0.5, 1, and 2 wt %). The XRD pattern of the parent zeolite as reported in our previous studies²³ displays that the nanozeolite Y was grown in the (111) and (733) planes, which is similar to another report.¹⁵ The pattern in this study exhibits the same peak position but with different intensities. This implies that addition of P does not alter the crystal structure, attributed to the amorphous form of P in the nanozeolite. The observed intensity reduction after addition of P was attributed to typical crystallinity loss and lattice defects as a result of dealumination.²⁴ Meanwhile, zirconium-modified nanozeolite Y shows a characteristic peak located around 34° , indicating the existence of ZrO_2 .²⁵ Additionally, the strong hydrolysis of zirconium in aqueous solution may destroy the zeolite structure to some extent.²⁰

The parent nanozeolite Y was also modified with metal, and the XRD pattern is shown in Figure 3. This XRD pattern exhibits different characteristics for parent and P-modified nanozeolites, which may be attributed to the different crystal

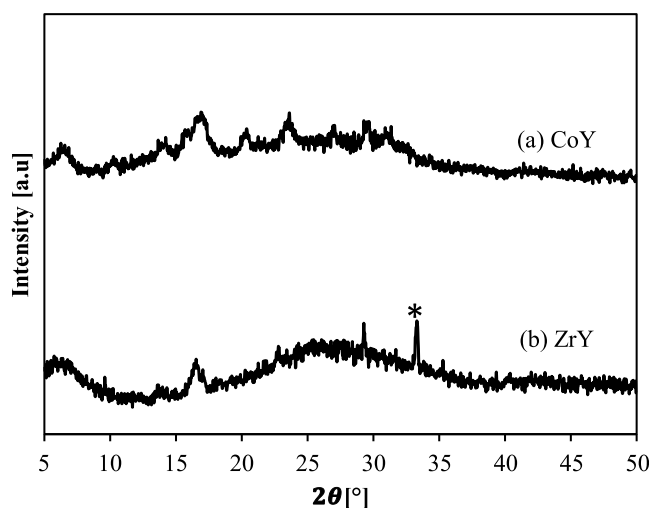


Figure 3. XRD pattern of metal-modified nanozeolite, (a) CoY and (b) ZrY.

structures. The nanozeolites modified with Co may transform to a cobalt–aluminate spinel after ion exchange.²⁶ Meanwhile, Zr^{4+} is a type of hard acid that is difficult to be exchanged with protons in the nanozeolite. Steaming and high temperature could help to penetrate into the framework but may result in uncontrolled distribution of metals inside the zeolitic framework.²⁷

The textural properties of the catalysts were elucidated with nitrogen adsorption–desorption, and the results are presented in Figure 4a and tabulated in Table 2. The adsorption–desorption pattern of the catalysts followed type V isotherms according to the IUCPAC classification with hysteresis. The pore size distributions of the catalysts as presented in Figure 4b were dominantly in the range of 3–6 nm, which agrees to the N_2 adsorption–desorption isotherm. The introduction of 0.5 wt % P decreased the surface area and pore volume significantly. This phenomenon occurs probably due to pore blockage and significant loss of crystallinity, as could be inferred by XRD patterns. Then, at a higher content of P (1.5 wt %), the external surface area is higher than that of the parent zeolites with decreasing trends of pore size. This is an indication of the excessive amount of P deposited in the nanozeolite surface after blocking some internal pores. Finally, at a higher content of P (2 wt %), the surface area and pore volume increased again, which might be due to the deposition of P on the surface of the nanozeolite. Meanwhile, for the metal-modified nanozeolite, the crystal transformation to spinel after Co modification caused reduction of the surface area, as reported by Wang et al.²⁸ In addition, the ion exchange with Zr at high calcination temperature may cover the zeolite surface or pore structure²⁹ with loss of the zeolite structure as evidenced by XRD.

The nature of the catalyst acidity was determined with ammonia temperature-programmed desorption (NH_3 -TPD) in the range of 125 – $625 \text{ }^\circ\text{C}$. Typically, the acid strength could be deduced by desorption temperature, which was divided into three categories, namely, 200, 200–400, and $400 \text{ }^\circ\text{C}$ corresponding to weak, medium, and strong acid, respectively. In this study, the desorption peak centered at around 200–400 $^\circ\text{C}$ presented in Figure 5 indicates the medium acid site. The peak area of the catalysts was 465, 571, 796, and $806 \mu\text{mol/g}$ for P, P1, P2, and P3, respectively. The introduction of P

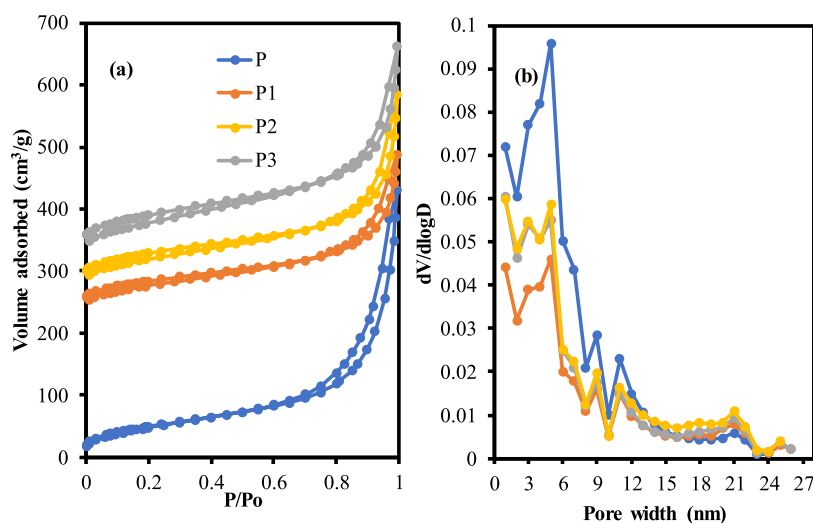


Figure 4. (a) N_2 adsorption–desorption isotherm and (b) pore size distribution of parent and phosphorous-modified nanozeolite Y.

Table 2. Textural Properties of the Catalysts

catalysts	surface area (m ² /g)	external surface area (m ² /g)	pore volume (cm ³ /g)	pore size (Å)
P	278	204	0.68	197
P1	247	181	0.38	126
P2	277	205	0.47	141
P3	301	243	0.50	156
ZrY	47	40		
CoY	61	50	0.03	93

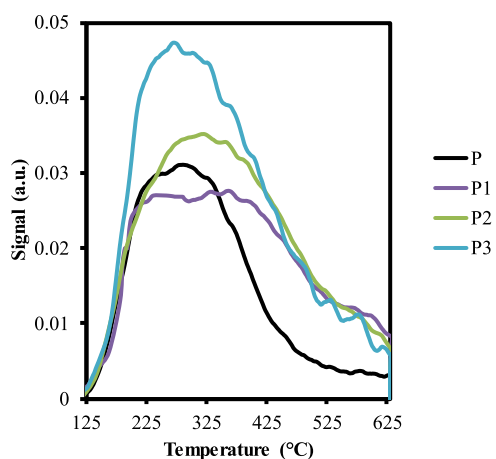


Figure 5. NH_3 -TPD profile of parent and phosphorous-modified nanozeolite Y.

clearly increased the overall acidity of the catalyst. However, the maximum P content (2 wt % P) comprises a less acidic site with similar total acidity compared to 1.5 wt % P, unlike significant acid evolution after addition of 1 and 1.5 wt % P. This phenomenon occurs due to alteration of the P structure with phosphate polycondensation at a high amount of P, as we will discuss in the NMR section.³⁰

Nuclear magnetic resonance (NMR) is a tool to estimate the atom position in a certain framework. Figure 6a shows the ²⁷Al MAS spectra of the parent and modified nanozeolites. The parent nanozeolite exhibits strong and low signals at around 60 and 6 ppm, respectively. These two peaks are attributed to tetrahedrally and pentahedrally coordinated Al in the zeolitic

framework. Then, when the parent nanozeolite was modified with phosphorous, there was a new peak at 0 ppm, which was assigned to the octahedrally coordinated framework. The introduction of 0.5 wt % P increased the peak at 60 ppm significantly, implying the increase of Al in the tetrahedral framework. However, at a higher P content (1 and 2 wt % P), the amount of Al in the tetrahedral framework decreased and transformed to octahedral Al, as indicated by the new peak at 0 ppm. The existence of aluminum phosphate may cause zeolite dealumination, as it formed after the removal of tetrahedral Al and in the absence of octahedral Al before P modification.³¹

The nature of P in nanozeolite Y at various contents was observed with ³¹P MAS NMR. There are several possibilities for the phosphorous location in the zeolite. P could be incorporated to the zeolitic framework with acid protonation with the zeolite hydroxyl group or interaction with the surface aluminum framework as presented in Figure 6b. Generally, there are three categories of P location, namely, P end chain, middle group and polymeric phosphate chains, and condensed phosphate chains located at −6, −14, and −23 ppm, respectively.³² In this study, only peaks at −14 and −23 ppm were observed as presented in Figure 6b. Then, the magnification of the chemical shift ranging from −15 to −25 ppm evidenced shifting and different peak intensities, as can be seen in Figure 6c. This was attributed to the P species as middle group and polymeric phosphate chains. With increasing content of P from 0.5 to 2 wt %, the intensified peak at 18.90 ppm δ indicated the increase of the middle group site due to more severe hydrolysis of phosphate acid that aligns with the ²⁷Al NMR result. From this NMR result, it could be deduced that the structure of the P-modified nanozeolite is as presented in Figure 6d.³³

3.2. Catalytic Evaluation of Nanozeolite Y. The *n*-dodecane conversion over nanozeolite Y and modified nanozeolite Y at different temperatures is shown in Figure 7a. There are two product phases in this reaction, namely, gas and liquid fractions. The remaining *n*-dodecane in the liquid fraction is indicated as unconverted feed in Tables 3 and 4. The parent nanozeolite Y showed higher conversion than that of all modified nanozeolites at 550 °C. Then, increasing temperature to 600 °C caused a significant increase of *n*-dodecane conversion to 97% with phosphorous-modified nanozeolite Y (1.5 wt % P). The *n*-dodecane conversion was

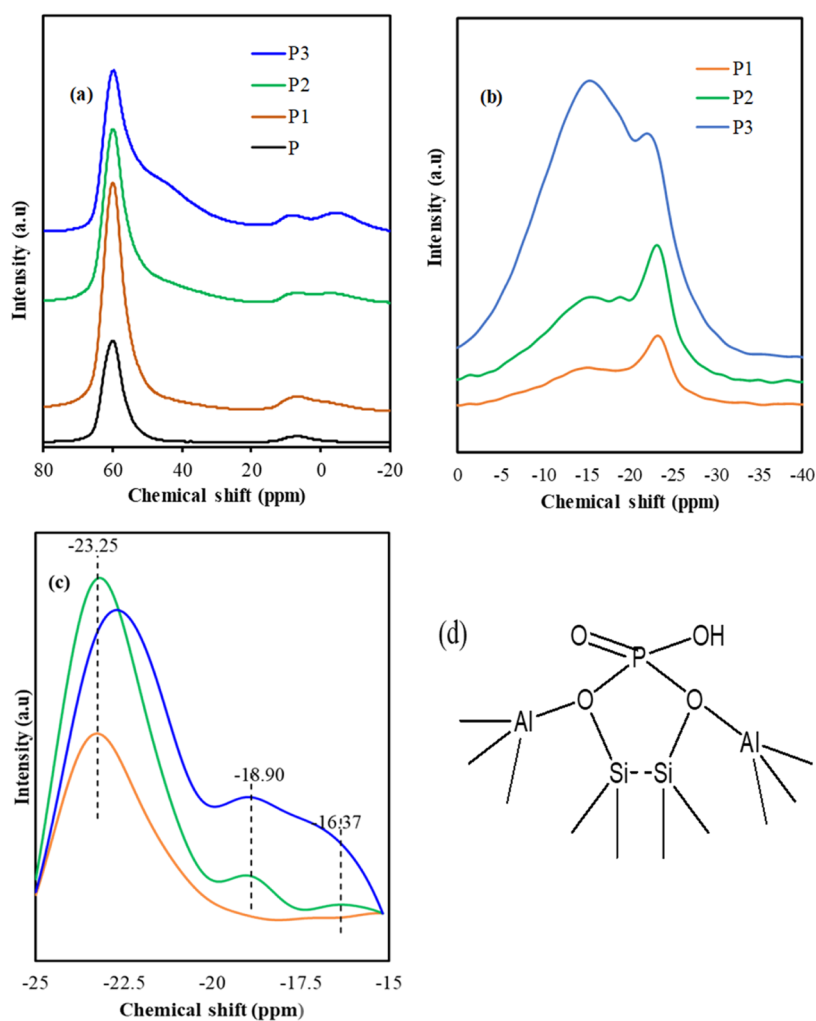


Figure 6. (a) ^{27}Al MAS NMR, (b) ^{31}P MAS NMR, and (c) magnification of ^{31}P MAS NMR at -25 to -15 ppm of parent and phosphorous-modified nanozeolite Y and (d) proposed structure of phosphorous-modified nanozeolite Y.

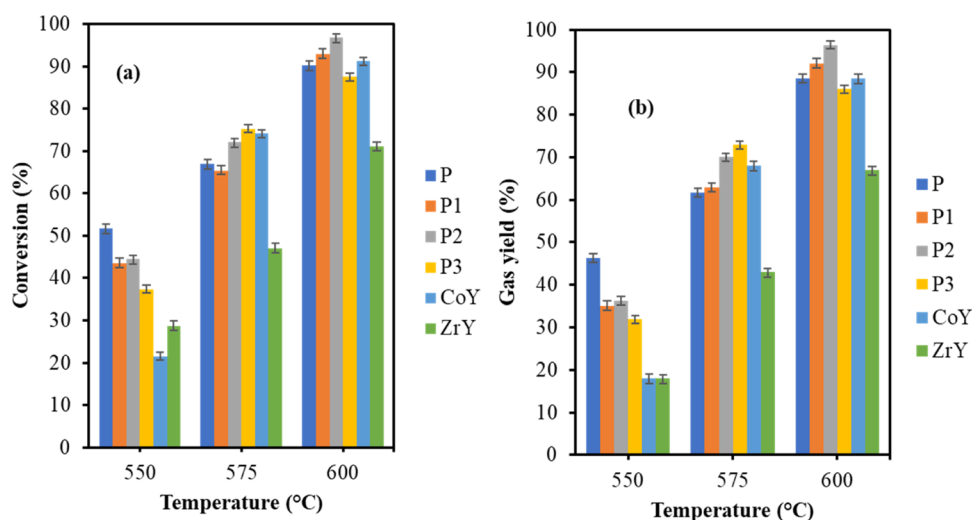


Figure 7. (a) *n*-Dodecane conversion and (b) gas yield at several temperatures.

then decreased with the introduction of 2 wt % P as a result of P removal during steam cracking of *n*-dodecane, as also reported by Yamaguchi et al.³⁴ Meanwhile, the Co embedded on nanozeolite Y showed similar activity as P-modified nanozeolite, as also reported to enhance activity in Fischer–

Tropsch synthesis.³⁵ As for Zr-modified nanozeolite Y, the catalytic activity decreased due to the existence of ZrO_2 damaging the zeolite structure to a certain extent as reported in XRD. The modification of zirconium resulted in higher

Table 3. Product Distribution of *n*-Dodecane Cracking with P-Modified Nanozeolite Y

product distributions	P1			P2			P3		
	550 °C	575 °C	600 °C	550 °C	575 °C	600 °C	550 °C	575 °C	600 °C
gas (wt %)	35.0	62.8	92.0	36.2	70.0	96.4	32.0	73.0	86.0
liq (wt %)	65.0	37.2	8.0	63.8	30.0	3.6	68.0	27.0	14.0
unconverted feed (wt %)	56.6	34.6	7.0	55.5	27.9	3.2	62.6	24.7	12.5
converted liquid (wt %)	8.5	2.6	1.0	8.3	2.1	0.4	5.4	2.3	1.5
conversion (wt %)	43.5	65.4	93.0	44.5	72.1	96.8	37.4	75.3	87.5
P/E (–)	0.7	1.0	0.7	0.7	0.5	0.4	0.6	0.5	0.5
olefins (wt %)	23.70	43.92	62.86	25.20	45.92	60.43	21.70	49.54	58.77
C ₂ ⁼ (wt %)	10.6	17.1	30.0	11.5	26.7	39.9	10.8	26.3	34.7
C ₃ ⁼ (wt %)	7.4	16.5	21.3	8.1	12.7	16.6	6.5	14.4	16.6
C ₄ ⁼ (wt %)	5.7	10.4	11.6	5.6	6.5	3.9	4.4	8.9	7.5
CH ₄ (wt %)	5.1	8.4	15.1	5.5	12.7	19.6	4.9	11.7	14.3
H ₂ (wt %)	1.5	3.0	5.1	1.9	4.0	6.7	1.9	4.0	5.8

Table 4. Product Distributions of *n*-Dodecane Cracking over Parent and Metal-Modified Nanozeolite Y

product distributions	P			CoY			ZrY		
	550 °C	575 °C	600 °C	550 °C	575 °C	600 °C	550 °C	575 °C	600 °C
gas (wt %)	46.3	61.6	88.6	18.0	68.0	88.6	18.0	43.0	67.0
liq (wt %)	53.7	38.4	11.4	82.0	32.0	11.4	82.0	57.0	33.0
unconverted feed (wt %)	48.3	33.0	9.8	78.5	25.9	8.8	71.3	53.0	29.0
converted liquid (wt %)	5.4	5.4	1.6	3.5	6.1	2.6	10.7	4.0	4.0
conversion (wt %)	51.7	67.0	90.2	21.5	74.1	91.2	28.7	47.0	71.0
P/E (–)	0.4	0.4	0.5	1.1	0.8	0.5	0.4	1.0	0.5
total olefins (wt %)	28.90	38.46	56.14	10.73	43.92	54.20	9.87	30.39	44.72
C ₂ ⁼ (wt %)	17.7	22.9	33.8	4.2	18.4	30.6	6.0	10.6	24.8
C ₃ ⁼ (wt %)	7.5	10.2	15.8	4.6	15.3	15.3	2.3	10.4	12.7
C ₄ ⁼ (wt %)	3.7	5.4	6.6	2.0	10.2	8.2	1.5	9.4	7.2
CH ₄ (wt %)	8.4	10.1	16.1	2.0	8.9	15.0	2.6	4.7	11.1
H ₂ (wt %)	2.5	2.8	4.6	2.1	7.4	10.9	0.8	2.3	4.9

conversion in catalytic cracking if it preserved the structure of the zeolite and dispersed homogeneously in the zeolite.^{20,36}

Similar trends with *n*-dodecane conversion were also observed for gas yield as presented in Figure 7b. The gas yield of the modified nanozeolite drastically increased at temperatures higher than 550 °C, with the P-modified nanozeolite. The higher total acidity of the P-modified nanozeolite might contribute to higher activity than that of parent nanozeolite Y, as also reported by Nasser et al.³⁷ The introduction of transition metals into the zeolite did not significantly impact the Brønsted acidity, but Lewis acidity increased with addition of metals. The newly formed Lewis acid acted as a new adsorption site of the formed olefins, while remaining paraffin adsorbed on Brønsted acid sites, thus increasing the olefin yield, if it preserved the zeolite structure after addition of metals.^{38,39}

The parent and modified nanozeolite Y exhibited a good olefin yield as presented in Figure 8a and Tables 3–4. The olefin yield of parent nanozeolite Y was ca. 30% at 550 °C, which increased to 38 and 55% at 575 and 600 °C, respectively. The olefin yield of P-modified nanozeolite Y increased to ca. 63% at 600 °C from ca. 23% at 500 °C. Meanwhile, metal-modified nanozeolite Y only slightly increased the olefin yield and reached a maximum value of 42% at 600 °C. The increasing olefin yield in the P-modified zeolite was also obtained in several reports.^{13,34} In terms of olefin distribution, the catalysts showed different behaviors at different temperatures. In general, the olefin distribution (Figure 8b) at all temperatures was ethylene > propene >

butenes, implying that nanozeolite Y preferred ethylene as indicated by the propene/ethylene (P/E) ratio, unlike BEA zeolites, which favored butenes.³⁷ Increasing temperature also increased the ethylene selectivity and reached an optimum value of ca. 40% with the introduction of 1 wt % P. To further understand the product distribution, the catalyst activities in terms of conversions, gas yield, olefin yield, and distribution are presented in Figure 8c at 575 °C as a representative trend. The optimum catalyst activity was for P2, signifying the importance of phosphorous modification to obtain a higher selectivity to olefins in *n*-dodecane-cracking systems.

4. CONCLUSIONS

In conclusion, nanozeolite Y was successfully synthesized and modified with phosphorous (P) and metals. At 550 °C, the modified nanozeolite Y has lower activity than the parent zeolite, but it changed to higher activity at higher temperatures. At first, phosphorous modifications resulted in higher catalytic activity than that of the parent nanozeolite and reached an optimum value with the addition of 1 wt % P. After that, the activity decreased due to the formation of aluminum phosphate and zeolite dealumination. Meanwhile, the Co-modified nanozeolite showed a similar catalytic behavior as parent nanozeolite Y but with a lower conversion and olefin yield compared to 1 wt % phosphorous-modified nanozeolite Y. Lastly, zirconium-modified nanozeolite Y exhibits lower activity due to damage of the zeolite structure to some extent and formation of ZrO₂.

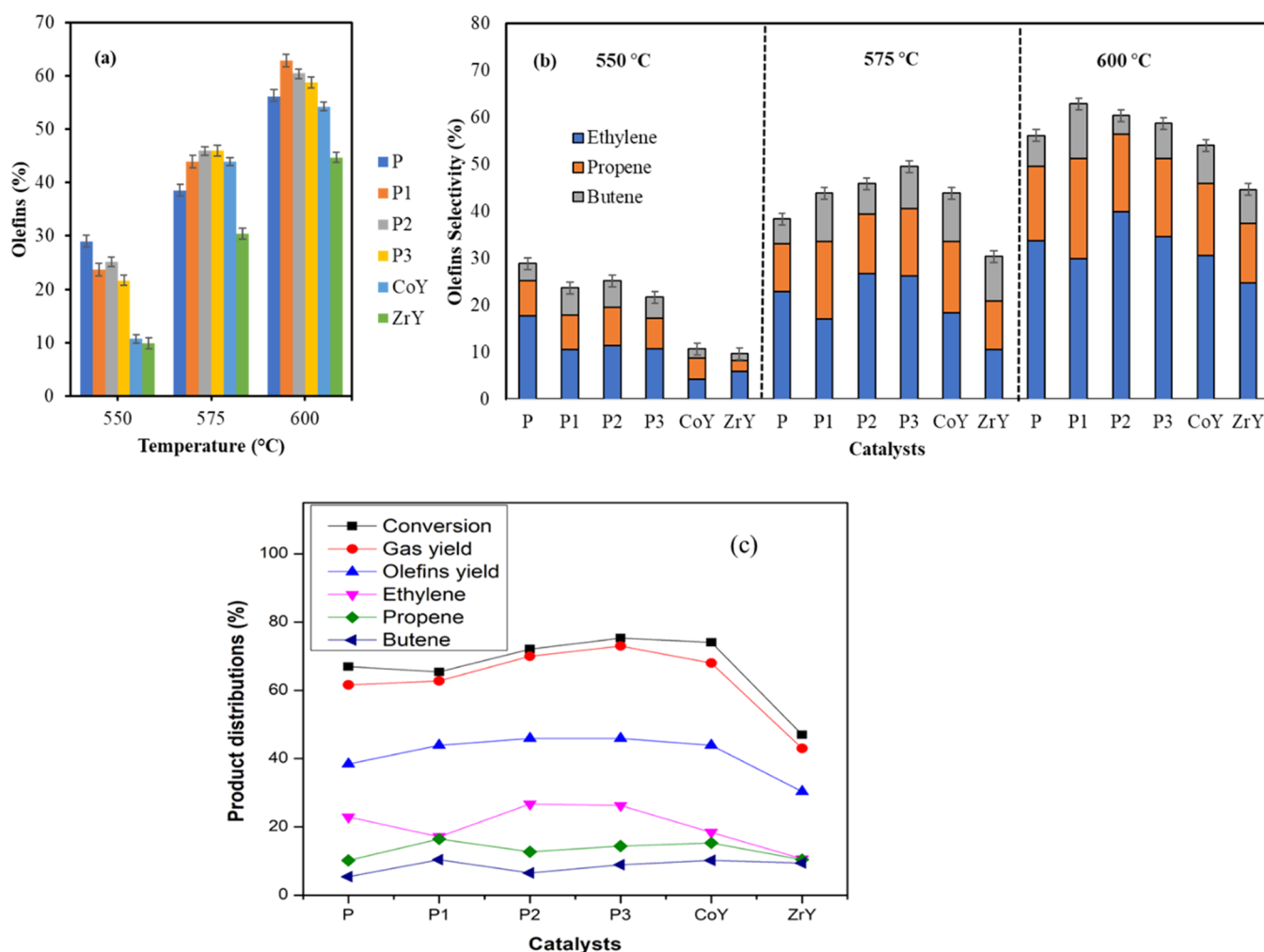


Figure 8. (a) Olefin yield (b) and olefin selectivity at several temperatures and (c) product distribution of the catalysts at 575 °C.

AUTHOR INFORMATION

Corresponding Author

Okı Muraza – Interdisciplinary Research Center for Hydrogen and Energy Storage and Chemical Engineering Department King Fahd University of Petroleum & Minerals, Dhahran 31261, Saudi Arabia; orcid.org/0000-0002-8348-8085; Email: omuraza@kfupm.edu.sa

Authors

Emad N. Al-Shafei – Research and Development Center, Saudi Aramco, Dhahran 31311, Saudi Arabia
Ahmad Masudi – Interdisciplinary Research Center for Hydrogen and Energy Storage and Chemical Engineering Department King Fahd University of Petroleum & Minerals, Dhahran 31261, Saudi Arabia
Zain H. Yamani – Interdisciplinary Research Center for Hydrogen and Energy Storage and Chemical Engineering Department King Fahd University of Petroleum & Minerals, Dhahran 31261, Saudi Arabia; orcid.org/0000-0002-6031-9385

Complete contact information is available at: <https://pubs.acs.org/10.1021/acsomega.2c02119>

Notes

The authors declare no competing financial interest.

ACKNOWLEDGMENTS

The authors would like to acknowledge the funding provided by Saudi Aramco under project No (CENT 2207) for Center of Research Excellence in Nanotechnology at King Fahd University of Petroleum & Minerals (KFUPM).

REFERENCES

- Masudi, A.; Jusoh, N. W. C.; Muraza, O. Opportunities for less-explored zeolitic materials in the syngas-to-olefins pathway over nanoarchitected catalysts: a mini review. *Catal. Sci. Technol.* **2020**, *10*, 1582–1596.
- Cordero-Lanzac, T.; Aguayo, A. T.; Gayubo, A. G.; Castano, P.; Bilbao, J. Simultaneous modeling of the kinetics for n-pentane cracking and the deactivation of a HZSM-based catalyst. *Chem. Eng. J.* **2018**, *331*, 818–830.
- Luo, M.; Hu, B.; Mao, G.; Wang, B. Trace Compounds Confined in SAPO-34 and a Probable Evolution Route of Coke in the MTO Process. *ACS Omega* **2022**, *7*, 3277–3283.
- Amghizar, I.; Vandewalle, L. A.; Van Geem, K. M.; Marin, G. B. New Trends in Olefin Production. *Engineering* **2017**, *3*, 171–178.
- Prantsidou, M.; Whitehead, J. C. The Chemistry of Gaseous Dodecane Degradation in a BaTiO₃ Packed-Bed Plasma Reactor. *Plasma Chem. Plasma Process.* **2015**, *35*, 159–172.
- Whitehead, J. C.; Prantsidou, M. Investigation of hydrocarbon oil transformation by gliding arc discharge: comparison of batch and recirculated configurations. *J. Phys. D: Appl. Phys.* **2016**, *49*, No. 154001.

- (7) Susanti, R. F.; Dianningrum, L. W.; Yum, T.; Kim, Y.; Lee, Y.-W.; Kim, J. High-yield hydrogen production by supercritical water gasification of various feedstocks: Alcohols, glucose, glycerol and long-chain alkanes. *Chem. Eng. Res. Des.* **2014**, *92*, 1834–1844.
- (8) Zhang, X.; Cheng, D.-g.; Chen, F.; Zhan, X. n-Heptane catalytic cracking on hierarchical ZSM-5 zeolite: The effect of mesopores. *Chem. Eng. Sci.* **2017**, *168*, 352–359. Ding, L.; Sitepu, H.; Al-Bogami, S. A.; Yami, D.; Tamimi, M.; Shaik, K.; Sayed, E. Effect of Zeolite-Y Modification on Crude-Oil Direct Hydrocracking. *ACS Omega* **2021**, *6*, 28654–28662.
- (9) Dauda, I. B.; Yusuf, M.; Gbadamasi, S.; Bello, M.; Atta, A. Y.; Aderemi, B. O.; Jibril, B. Y. Highly Selective Hierarchical ZnO/ZSM-5 Catalysts for Propane Aromatization. *ACS Omega* **2020**, *5*, 2725–2733.
- (10) Qamar, M.; Ahmed, M. I.; Qamaruddin, M.; Asif, M.; Sanhoob, M.; Muraza, O.; Khan, M. Y. A Mesopore-Dependent Catalytic Cracking of n-Hexane Over Mesoporous Nanostructured ZSM-5. *J. Nanosci. Nanotechnol.* **2018**, *18*, 5711–5720.
- (11) Konno, H.; Tago, T.; Nakasaka, Y.; Ohnaka, R.; Nishimura, J.-i.; Masuda, T. Effectiveness of nano-scale ZSM-5 zeolite and its deactivation mechanism on catalytic cracking of representative hydrocarbons of naphtha. *Microporous Mesoporous Mater.* **2013**, *175*, 25–33.
- (12) Mohammadparast, F.; Halladj, R.; Askari, S. The Crystal Size Effect of Nano-Sized ZSM-5 in the Catalytic Performance of Petrochemical Processes: A Review. *Chem. Eng. Commun.* **2015**, *202*, 542–556.
- (13) Ji, Y.; Yang, H.; Zhang, Q.; Yan, W. Phosphorus modification increases catalytic activity and stability of ZSM-5 zeolite on supercritical catalytic cracking of n-dodecane. *J. Solid State Chem.* **2017**, *251*, 7–13.
- (14) Hao, J.; Wang, Y.; Liu, G.; Zhang, J.; Li, G.; Ma, X. Synthesis of ITQ-2 Zeolites and Catalytic Performance in n-Dodecane Cracking. *Chin. J. Chem. Eng.* **2014**, *22*, 869–874.
- (15) Radman, H. M.; Dabbawala, A. A.; Ismail, I.; Alwahedi, Y. F.; Polychronopoulou, K.; Vaithilingam, B. V.; Singaravel, G. P.; Morin, S.; Berthod, M.; Alhassan, S. M. Influence of salt on nanozeolite-Y particles size synthesized under organic template-free condition. *Microporous Mesoporous Mater.* **2019**, *282*, 73–81.
- (16) Blasco, T.; Corma, A.; Martínez-Triguero, J. Hydrothermal stabilization of ZSM-5 catalytic-cracking additives by phosphorus addition. *J. Catal.* **2006**, *237*, 267–277. Chu, Y.; Gao, X.; Zhang, X.; Xu, G.; Li, G.; Zheng, A. Identifying the effective phosphorus species over modified P-ZSM-5 zeolite: a theoretical study. *Phys. Chem. Chem. Phys.* **2018**, *20*, 11702–11712.
- (17) Etim, U. J.; Xu, B.; Zhang, Z.; Zhong, Z.; Bai, P.; Qiao, K.; Yan, Z. Improved catalytic cracking performance of USY in the presence of metal contaminants by post-synthesis modification. *Fuel* **2016**, *178*, 243–252. Lee, J.; Hong, U. G.; Hwang, S.; Youn, M. H.; Song, I. K. Catalytic cracking of C5 raffinate to light olefins over lanthanum-containing phosphorous-modified porous ZSM-5: Effect of lanthanum content. *Fuel Process. Technol.* **2013**, *109*, 189–195. Ahmed, M. H. M.; Muraza, O.; Jamil, A. K.; Shafei, E. N.; Yamani, Z. H.; Choi, K.-H. Steam Catalytic Cracking of n-Dodecane over Ni and Ni/Co Bimetallic Catalyst Supported on Hierarchical BEA Zeolite. *Energy Fuels* **2017**, *31*, 5482–5490.
- (18) Deng, C.; Zhang, J.; Dong, L.; Huang, M.; Bin, L.; Jin, G.; Gao, J.; Zhang, F.; Fan, M.; Zhang, L.; et al. The effect of positioning cations on acidity and stability of the framework structure of Y zeolite. *Sci. Rep.* **2016**, *6*, No. 23382.
- (19) Tukur, N. M.; Al-Khattaf, S. Catalytic cracking of n-dodecane and alkyl benzenes over FCC zeolite catalysts: Time on stream and reactant converted models. *Chem. Eng. Process.: Process Intensif.* **2005**, *44*, 1257–1268.
- (20) Yu, S.; Yan, J.; Lin, W.; Zhang, J.; Long, J. Characterization and cracking performance of zirconium-modified Y zeolite. *Catal. Commun.* **2021**, *148*, No. 106171.
- (21) Kantarelis, E.; Javed, R.; Stefanidis, S.; Psarras, A.; Iliopoulou, E.; Lappas, A. Engineering the Catalytic Properties of HZSM5 by Cobalt Modification and Post-synthetic Hierarchical Porosity Development. *Top. Catal.* **2019**, *62*, 773–785.
- (22) Sanhoob, M. A.; Shafei, E. N.; Khan, A.; Nasser, G. A.; Bakare, I.; Muraza, O.; Al-Bahar, M. Z.; Al-Jishi, A. N.; Al-Badair, H. H.; Ummer, A. C. Catalytic Cracking of n-Dodecane to Chemicals: Effect of Variable-Morphological ZSM-5 Zeolites Synthesized Using Various Silica Sources. *ACS Omega* **2022**, *7*, 10317–10329.
- (23) Shafei, E. N.; Masudi, A.; Yamani, Z. H.; Muraza, O. Acidity modifications of nanozeolite-Y for enhanced selectivity to olefins from the steam catalytic cracking of dodecane. *RSC Adv.* **2022**, *12*, 18274–18281.
- (24) Zhao, G.; Teng, J.; Xie, Z.; Jin, W.; Yang, W.; Chen, Q.; Tang, Y. Effect of phosphorus on HZSM-5 catalyst for C4-olefin cracking reactions to produce propylene. *J. Catal.* **2007**, *248*, 29–37.
- (25) Rauta, P. R.; Manivasakan, P.; Rajendran, V.; Sahu, B. B.; Panda, B. K.; Mohapatra, P. Phase transformation of ZrO₂ nanoparticles produced from zircon. *Phase Transitions* **2012**, *85*, 13–26.
- (26) Beale, A. M.; Sankar, G. Understanding the Crystallization of Nanosized Cobalt Aluminate Spinel from Ion-Exchanged Zeolites Using Combined in Situ QEXAFS/XRD. *Chem. Mater.* **2006**, *18*, 263–272.
- (27) Kosinov, N.; Liu, C.; Hensen, E. J. M.; Pidko, E. A. Engineering of Transition Metal Catalysts Confined in Zeolites. *Chem. Mater.* **2018**, *30*, 3177–3198.
- (28) Wang, C.; Liu, S.; Liu, L.; Bai, X. Synthesis of cobalt–aluminate spinels via glycine chelated precursors. *Mater. Chem. Phys.* **2006**, *96*, 361–370.
- (29) Díaz, E.; Ordóñez, S.; Vega, A.; Coca, J. Catalytic combustion of hexane over transition metal modified zeolites NaX and CaA. *Appl. Catal., B* **2005**, *56*, 313–322. Zhu, L.; Lv, X.; Tong, S.; Zhang, T.; Song, Y.; Wang, Y.; Hao, Z.; Huang, C.; Xia, D. Modification of zeolite by metal and adsorption desulfurization of organic sulfide in natural gas. *J. Nat. Gas Sci. Eng.* **2019**, *69*, No. 102941.
- (30) Li, X.; Qiao, K.; He, L.; Liu, X.; Yan, Z.; Xing, W.; Qin, L.; Dai, B.; Zhang, Z. Combined modification of ultra-stable Y zeolites via citric acid and phosphoric acid. *Appl. Petrochem. Res.* **2014**, *4*, 343–349.
- (31) Souza, E. C. d.; Pereira, M. M.; Lam, Y. L.; Morgado, E.; Chinelatto, L. S. Aluminum phosphate as active matrix of fluid catalytic cracking catalysts: Y zeolite stabilization. *Appl. Catal., A* **2021**, *619*, No. 118156.
- (32) Göhlich, M.; Reschetilowski, W.; Paasch, S. Spectroscopic study of phosphorus modified H-ZSM-5. *Microporous Mesoporous Mater.* **2011**, *142*, 178–183.
- (33) Zhao, P.; Boekfa, B.; Nishitoba, T.; Tsumoji, N.; Sano, T.; Yokoi, T.; Ogura, M.; Ehara, M. Theoretical study on 31P NMR chemical shifts of phosphorus-modified CHA zeolites. *Microporous Mesoporous Mater.* **2020**, *294*, No. 109908.
- (34) Yamaguchi, A.; Jin, D.; Ikeda, T.; Sato, K.; Hiyoshi, N.; Hanaoka, T.; Mizukami, F.; Shirai, M. P-ZSM-5 Pretreated by High-Temperature Calcination as Durable Catalysts for Steam Cracking of n-Hexane. *Catal. Lett.* **2014**, *144*, 44–49.
- (35) Liu, J.-Y.; Chen, J.-F.; Zhang, Y. Cobalt-embedded zeolite catalyst for direct syntheses of gasoline via Fischer–Tropsch synthesis. *Catal. Sci. Technol.* **2013**, *3*, 2559–2564. 10.1039/C3CY00458A
- (36) Momayez, F.; Towfighi Darian, J.; Teimouri Sendesi, S. M. Synthesis of zirconium and cerium over HZSM-5 catalysts for light olefins production from naphtha. *J. Anal. Appl. Pyrolysis* **2015**, *112*, 135–140.
- (37) Nasser, G. A.; Ahmed, M. H. M.; Firdaus, M. A.; Sanhoob, M. A.; Bakare, I. A.; Al-Shafei, E. N.; Al-Bahar, M. Z.; Al-Jishi, A. N.; Yamani, Z. H.; Choi, K.-H.; Muraza, O. Nano BEA zeolite catalysts for the selective catalytic cracking of n-dodecane to light olefins. *RSC Adv.* **2021**, *11*, 7904–7912.
- (38) Rahimi, N.; Karimzadeh, R. Catalytic cracking of hydrocarbons over modified ZSM-5 zeolites to produce light olefins: A review. *Appl. Catal., A* **2011**, *398*, 1–17.

(39) Wang, L.; Peng, B.; Zheng, A.; Song, Y.; Jiang, Q.; Song, H.; Lin, W.; He, M. Origin of Enhanced Ethylene Yield: Differentiated Alkene Adsorption in the Alkane Cracking. *SSRN Electron. J.* **2022**, No. 4112475.